# EFFECT OF TIME VARIATION ON STRUCTURAL / OPTICAL PROPERTIES OF ALUMINIUM DOPED MANGANESE OXIDE THIN FILMS

Supported by tetfund

**Okpechi K.U.P[1], Nwaokorongwu E.C[2], Joseph U[3]**
[1,2,3](Department of Physics, Michael Okpara University of Agriculture, Umudike, Umuahia, Abia State, Nigeria)
Corresponding Author: chiemeriedalu@gmail.com

**Received:** September 14, 2023 **Accepted:** November 28, 2023

**Abstract:** Manganese oxide thin films were doped with10% Aluminum (Al) on glass substrates at deposition temperature of 55°C using the successive ionic layer adsorption reaction (SILAR) method with NaOH as source of $OH^-$. The films were annealed at 300°C using the master chef annealing machine and the times for the deposition were varied for 1hr, 1hr.15mins. 1hr.30mins, 1hr.45 mins and 2hrs. The crystallographic studies were done using X-ray diffractometer. All the films were found to be polycrystalline in nature. The optical characteristics of the thin film were studied using UV-1800 double beam spectrophotometer. The films show very high transmittance and low absorbance in the visible infrared region of the electromagnetic spectrum. The band gaps of the films were calculated from absorption coefficient results. From the spectral observations, these films may not be good material for use as solar cell collectors but may be very useful as solar cell collector cover, anti–reflection in smart windows, parasitic capacitance, and composite materials in electrical and electronic devices.

**Keywords:** SILAR, Manganese Oxide, thin films, XRD.

## Introduction

Many researchers have synthesized and studied the properties of nanosized materials in the recent years. These interesting properties such as catalytic, thermal, magnetic, electrical and optical properties and the variety of applications related to them have brought them to the limelight in research and modern technology. Manganese oxide thin films are an important class of materials which exhibit very interesting properties for uses in high-density magnetic storage media, catalysts, solar energy, molecular adsorption, varistors and more (Ilya *et al.*, 2021). Moreso, MnO and $MnO_2$ nanomaterials have been of great interest as anode materials in lithium-ion batteries (LIBs) due to their high theoretical capacity, low cost, environmental benignity, and other special properties when doped with semiconductor elements, such as, Aluminum, Tin, zinc, iron, Cobalt, Nickel, etc. (Rajesh *et al.*, 2018). Replacing Manganese with these metals improves its stability. $Al^{3+}$ shows good doping potential due to the similar radius towards $Mn^{3+}$ (Chougule *et al.*, 2012). The phases, sizes, and morphologies of Al doped MnO [AlMnO] thin films have great effect on the properties and applications of the material; there has been ongoing research on the control of phase, shape, size, and dimensionality of these thin films in recent years (Ilya *et al.*, 2021; Rajesh *et al.*, 2018; Chougule *et al.*, 2012). Several effective deposition methods have been devoted to prepare manganese oxides thin film materials with various shapes and excellent properties, such as hydro-thermal technique (Guotai *et al.*, 2019), Sol–gel technique (Muslim and Jiban, 2020), electro-chemical deposition method (Ozkan *et al.*, 2018), chemical bath (Mishra *et al.*, 2018), and spray pyrolysis technique (Su *et al.*, 2014), SILAR (Sahay *et al.*, 2017)].

The aim of this paper is to develop and study new manganese oxide doped with Aluminum materials synthesized by Successive Ionic Layer Adsorption Reaction (SILAR) method and to observe the effects of time variation during annealing on the optical and structural property of the Al doped manganese oxide thin films. SILAR technique has several advantages over the others such as low cost, safety and easy handling. It does not require vacuum conditions, and by employing different deposition parameters, the microstructure and surface morphology of the films can be controlled (Ozkan *et al.*, 2018; Mishra *et al.*, 2018).

## Computational Methodology/Materials & Methods

Al doped MnO[AlMnO] thin films were deposited by mixing a molar solution of manganese chloride and aluminum chloride with Ammonia NH4 and Ethylene diamine tetraacetate ($Na(C_{10}H_{16}N_2O_8)$) commonly known as EDTA as complexing agents. For the deposited sample, $MnCl_2.6H_2O$ was a source of manganese. 10mls of MnCl containing 40g of 0.6M of MnCl was added to 3ml of 3M of $NH_4$ and 10% of $AlCl_2$ was introduced as dopant into the complex solution of ($NH_4$) MnCl. 3mls of EDTA was also added to increase the solution stability forming a white ppt solution, and distilled water was used to complete the solution to 50mls. Distilled water was also used as the ion exchange water to remove loose particle from the substrate. 30mls of NaOH containing 37.2g of 0.5M of NaOH also was used to complete the cycle and as a source of OH ion to form MnO. The pH value of the solution was 9.0. The adsorption to the substrate was gotten after an increased in the deposition temperature, using a temperature bath of 55°C. The dip time in each reactant was 20secs in cationic precursor AlMnO solution, 5secs in distilled water and 20secs in anionic NaOH solution. The number of cycles was 20 cycle to enhance the deposition. Five samples of AlMnO films were fabricated using Successive Ionic Layer Adsorption Reaction [SILAR] method and were annealed at a constant temperature of 300°C with varied time of 1hr, 1.30hrs, 1.45hrs, 2.00hrs, for further characterization.

## Results and Discussion

The structural properties were studied using X-ray diffraction (XRD), a basic method for determining the crystalline structure of samples. The analysis of XRD is usually based on the principles of constructive and destructive interferences of monochromatic X-rays and a crystalline sample. The X-rays are produced by a cathode ray tube, sieved to produce

monochromatic radiation, collimated to concentrate, and focused toward the sample. The interaction of the incident rays with the sample produces constructive interference (and a diffracted ray) when conditions satisfy Bragg's law.

$n\lambda = 2d \sin\theta$ 1

Where, $\theta$ is the angle of diffraction between the primary X-ray beam (with $\lambda$ as wavelength),
d is the interplanar spacing;
and n is an integer.

This law relates the wavelength of an electromagnetic radiation to the diffraction angle and the lattice spacing in a crystalline sample. X-ray diffractometer modeled GBC Enhanced Mini Material Analyzer (EMMA) was used in analyzing the material. It gives information relating to the nature and structure of the doped thin films of AlMnO. The crystallite size was obtained by the resolution of Scherrer's equation:

$D_{(hkl)} = \frac{K\lambda}{B\cos\theta}$ 2

Where:
$D(hkl)$): The average crystallite or particle size in a direction of plane (hkl) (nm)
λ: The X-ray wavelength (nm) Where λ is the wavelength of Cu-K radiation (λ =1.54060 0A)
*K:* A dimensionless shape factor ($K$ = 0.94)
B: Full Width at Half Maximum (FWHM) of the diffraction peak (rad)
θ: Bragg diffraction angle (deg)

The lattice parameter which refers to the physical dimension of unit cells in a crystal lattice with three lattice constants for three dimensional lattices denoted by a b, c for the thin films was calculated for different phases of the materials deposited.

Hexagonal phase formula:

$$\frac{1}{d^2} = \frac{4}{3}\left(\frac{h^2 + hk + k^2}{a_o^2}\right) + \frac{l^2}{c_o^2} \quad 3$$

For cubic phase, the lattice constant was calculated from

$\frac{1}{d^2} = \frac{h^2+k^2+l^2}{a}$ 4

Where d is the interplaner distance and hkl is the miller indices.

For tetragonal phase of the crystal structure $\frac{1}{d} = \frac{h^2+k^2}{a^2} + \frac{l^2}{c^2}$ 5

The micro strain was calculated using:

$\varepsilon = \frac{\beta\cos\theta}{4}$ 6

The dislocation density (d) was determined using

$\partial = \frac{1}{D^2}$ 7

where d is the crystallite size

The volume for simple cubic was calculated from

$V = a^3$ 8

For hexagonal structure

$V = \frac{\sqrt{3}a^3c}{2}$ 9

For tetragonal structure

$V = a^2c$ 10

***Optical Measurements***

The optical properties of the thin films are defined by the interaction between is electromagnetic radiation (light) and the material, including absorption, diffraction, polarization, reflection, refraction and scattering effects. The measurements are simple to perform as long as a satisfactory spectroscopic apparatus is available in the wavelength region of interest. In this work, the optical performances of the thin films, which essentially consist of the absorbance, transmittance and reflectance, were studied using UV1-1800 series double beam spectrophotometer. The absorbance of the deposited films was measured using UV-spectrophotometer and occurred in the spectral range of 300nm-900nm of the electromagnetic spectrum. Other spectral/Optical parameters such as transmittance, reflectance, etc. were estimated using appropriate mathematical formulas.

***Transmittance***

The values of absorbance were converted to transmittance using:

%T=antilog (2-absorbance) 11

***Reflectance (R)***

The reflectance was estimated using the equation (He and Ling, 2011).

1=A+T+R 12

Where A is the absorbance, T is the transmittance and R is the reflectance of the deposited films.
For normalization, equation 12 becomes

$R1 = -(T + R)$ 13

***Absorption coefficient (α)***

Absorption co-efficient is the fractional decrease in intensity of radiation per unit increase in distance (Sina *et al.*, 2023). When a beam of electromagnetic radiation $\mathbf{I_o}$ is incident on a thin film surface, then

$I=I_oe^{-\alpha t}$ 14

Where t is the distance travelled by the radiation and I is the radiation intensity of thickness.
But equation 14 can be written as

$I/I_o=e^{\alpha t}$ 15

From equation 15, it becomes

$1/T= e^{\alpha t}$ 16

Taking the natural log of the equation 16 becomes

$Ln(1/T)=\alpha t$ 17

For a unit distance, equation 17 becomes

$Ln(1/T)=\alpha$ 18

Therefore, the absorption coefficient is;

A = LN (1/T) 19

Equation 19 was used to deduce the absorption coefficient of the thin film.

***Optical energy band gap ($E_g$)***

The relationship between the absorption coefficient (α) and incident photon energy (hν) can be determined using the well-known Tauc's relations (Chougule *et al.*, 2012; Jaml *et al.*, 2017).

$(\alpha h\nu) = A\,(h\nu - E_g)^n$ 20

Where v is the frequency of the incident photon, h is the Planck's constant, A is a constant, $E_g$ is the optical band gap and n is the transition type.

It has been established that for direct allowed band gap semiconductors, the measured absorption data fits well to equation (20) for $n = {}^1/_2$. $(\alpha h\nu) = A\,(h\nu - Eg)^{1/2}$ 21

Taking the square of both sides of equation 21, we have

$(\alpha h\nu)^2 = A(h\nu - E_g)$ 22

Hence, the graph of $(\alpha h\nu)^2$ against h$\nu$ was plotted and values of optical band gap energies $E_g$ were obtained from extrapolating the straight portion of the graphs on the photon energy (h$\nu$) axis at $(\alpha h\nu)^2 = 0$.

***Extinction coefficient (k)***

The extinction coefficient (k) of the films was determined using the equation for semi-conductors and insulators (Sina *et al.*, 2023).

$$K = \alpha\lambda/4\pi \quad (23)$$

Where α is the absorption coefficient of the thin film and λ is the wavelength of the incident electromagnetic radiation.

***Refractive index (n)***

The relationship between the index of refraction ($n_s$) and the film reflectance (R) was used to estimate the refractive index (Gao *et al.*, 2014; Salek *et al.*, 2015);

$$R = (n_s-1)^2/(n_s+1)^2 \quad (24)$$

Equation 24 is simplified

$$n=(1+(R)^{1/2})/(1-(R)^{1/2} \quad (25)$$

***Dielectric constant (ε)***

The complex dielectric constant (ε) is given by;

$$\varepsilon = \varepsilon_r + \varepsilon_i = (n + jk)^2 \quad (26)$$

Where $\varepsilon_r$ = real part, $\varepsilon_i$ = imaginary part, n =refractive index and k = extinction coefficient.

Expanding equation 26, we obtain;

$$\varepsilon = \varepsilon_r + \varepsilon_i = (n^2 - k^2) + 2njk$$

Equating the real and imaginary parts of the equation (26) we have that,

$$\varepsilon_r = (n^2 - k^2) \text{ (The real part)} \quad (27)$$

$$\varepsilon_i = 2nk \text{ (The imaginary part)} \quad (28)$$

***Optical conductivity ($\sigma_o$)***

The optical conductivity was estimated by the equation;

$$\sigma_o = \alpha nc/4\pi \quad (29)$$

Where c is the speed of light in vacuum, α is the absorption coefficient and n is the index of refraction of the film.

***XRD results***

The XRD pattern of AMO are shown for films annealed for 1hr and 2hrs. each pattern can be indexed to a body centered tetragonal phase ( JCPDS card no: 44-0141). The strongest peaks were seen at (211)(301) crystal planes with $2\theta = 38^o$ and $40^o$. Peaks of Aluminuim pattern were also seen at $2\theta = 34.2^o$, with its corresponding hkl at (0 1 2). The lattice constant paramaters, volume, microstrian and dislocation density were reported in Table 1 with the lattice constant increasing with increase in annealing time.

The particle morphology was examined by direct observation using scanning eletron microscope (SEM). In Figs.2a and 2b, the particle is made up of many smaller grains which could correspond to the crystalite size determined by XRD. Similar morphology for $Co_2MnO_4$ and $Ni_{0.2}Co_{1.4}Mn_{1.4}O_4$ was also reported (Park *et al.*, 2013; Winm, 2012).

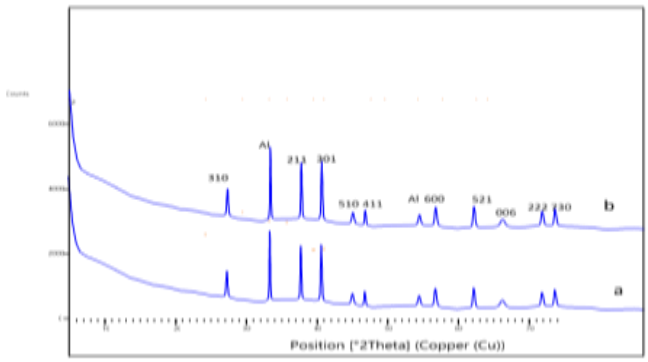


**Fig.1** XRD peaks for AMO thin films annealed for (a)1hr and (b) 2hrs

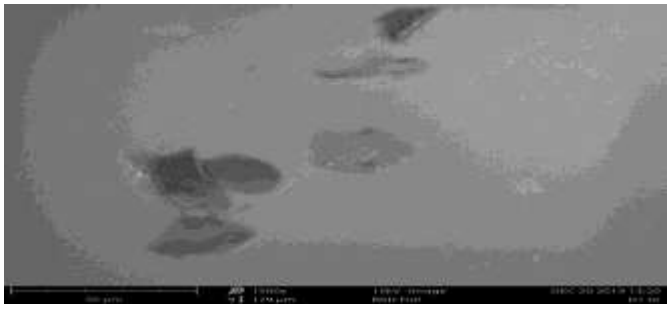

**Fig.2a** SEM Micrograph for AMO thin films annealed at 300°C for 1hr

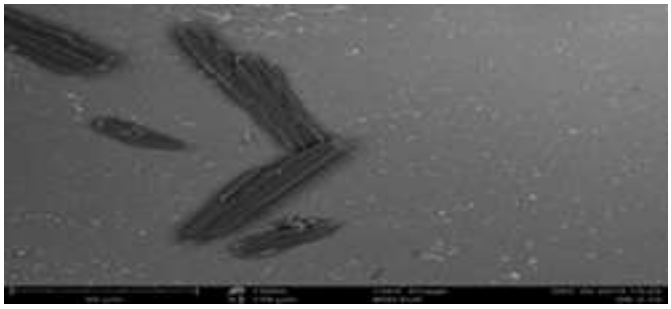

**Fig.2b** SEM Micrograph for AMO thin films annealed at 300°C for 2hrs

**Table 1** XRD Parameters of AlMnOannealed at 1hr and 2hrs

| Samples | Average crystal size | Lattice constant Å | Lattice constant b | Dislocation density δ | Micro strain ε | Volume, V ($cm^3$) |
|---|---|---|---|---|---|---|
| 1hr | 1.765 | a=1.01143 | 1.9823 | 0.56642 | 1.8575 | 2.02787 |
| 2hrs | 2.276 | a=2.4311 | 2.2653 | 0.56875 | 2.0987 | 3.06788 |

***Optical Properties***

Table 2 explain the sample codes used in the sample graphs. Figure 3 shows absorbance of the AMO thin films which were generally low at about 0.8 at wavelength of 350 nm for the film that was not variedbut decreases to 0.2 with increased wavelength of 400nm in the UV region of the spectrum with increase in varying time. Figure 4 shows a high transmittance of 65% to 100% was observed in the

range of 300nm to 800nm of the UV-visible region of the spectrum. This high transmittance confirmed the AMO could be used inglass coating for use in flate plate collectors application. Figure 5 shows the plot for reflectance with a uniform peak reflectance at 20% at the wavelength of 330nm in the UV region of thespectrum.which shows a low reflectivity of the material. The reflectance reduced drastically along the visible region of the spectrum. Figure 6 shows the optical band gap which was determined by extrapolation of the linear portion of the peaks for each plot of $(\alpha h\nu)^{1/2} = 0$. A band gap of 4.2 was observed in the film that was kept constant (reference film) but drops to 4.0 as the annealing time was varied. This is in line with the theory that annealing reduces the value of bandgap. It was also observeved from the graph that the annealing time did not affect the bandgap of the thin films, as the films appears to be constant all through the varied time. The bandgap shift to lower energies can be as a result of the carrier confinement in the small semiconductor particles or as a result of increase in annealing time of the thin films. From previous research work, observations of a band gap of 0.98 ev in an ă- MnO nanowires was observed (Salek *et al.*, 2015). Moreso, bandgap of 1.32eV in ă - $MnO_2$ nanofibers was reported (Sina *et al.*, 2023), MnO nanosheet with a bandgap of about 2.23eV was also reported (Wim, 2012), from Fig.7, the refractive index is in the range of 1.22 and 1.25 in the photon energy of 4.0 eV. Figure 8 is the optical conductivity which increased with increasE in time. Figures 9 and 10 reveal the dielectric constant, the films had very low dielectric, decreasing with increase in annealing time. The extinction coefficient was observed in Fig.11 which also decrease with increase in annealing time. Figure 12 explains the absorption coefficient of the thin film which shows that the rate of absorption of light is poor in Al doped MnO thin films, and decreased with increase in annealing time.

**Table 2** Sample codes for the thin film materials deposited

| Sample code | Time variation |
|---|---|
| $D_0$ | 0hr (reference) |
| D2 | 1hr |
| D3 | 1hr.30mins |
| D4 | 1hr.45mins |
| D5 | 2hrs |

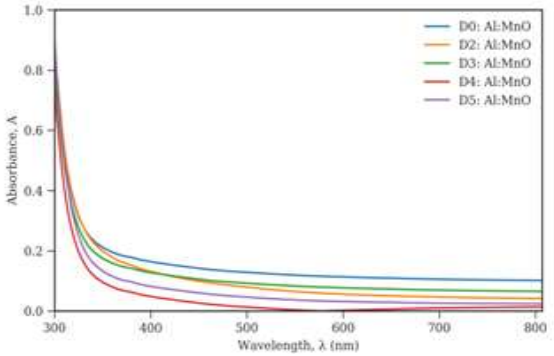


**Fig.3** Plot of absorbance versus wavelength for AMO thin film annealed at 300°C for varying time

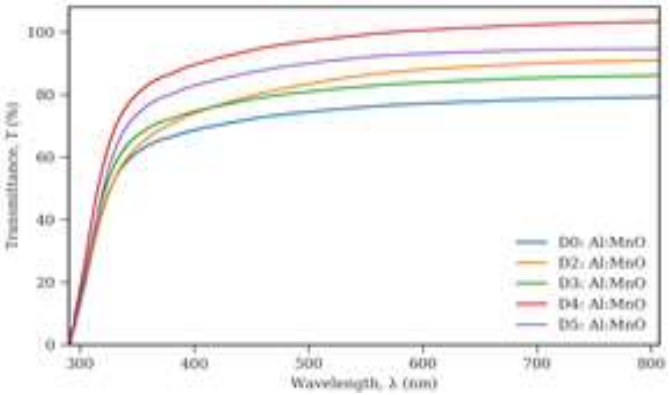


**Fig.4** Plot of transmittance versus wavelength for AMO thin film annealed at 300°C for varying time

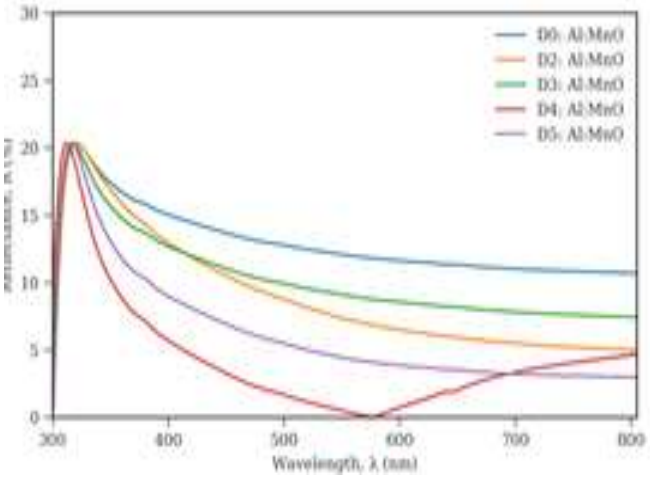


**Fig.5** Plot of reflectance versus wavelength for AMO thin film annealed at 300°C for varying time

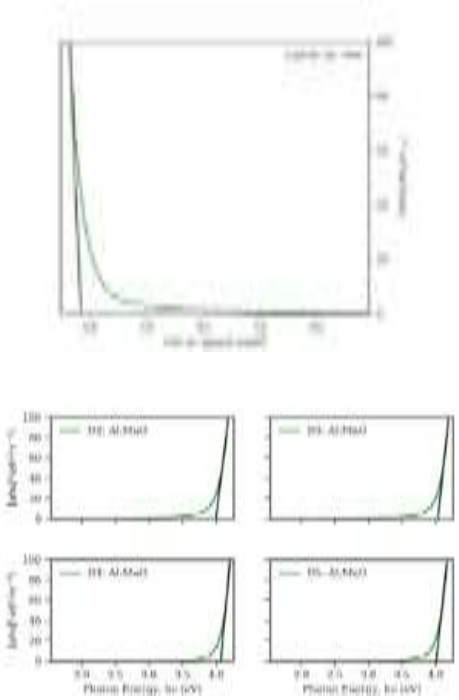

**Fig.6** Plot of band gap versus photon energy for AMO thin

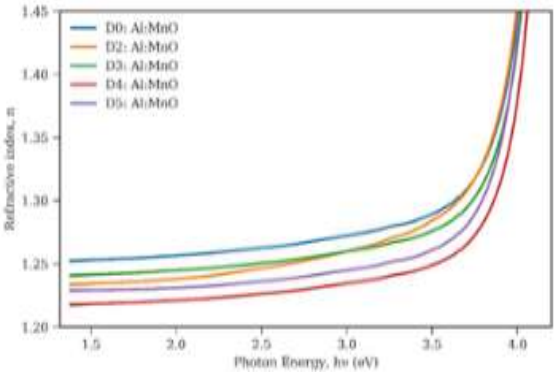


**Fig.7** Plot of refractive index versus photon energy for AMO thin film annealed at 300°C for varying time

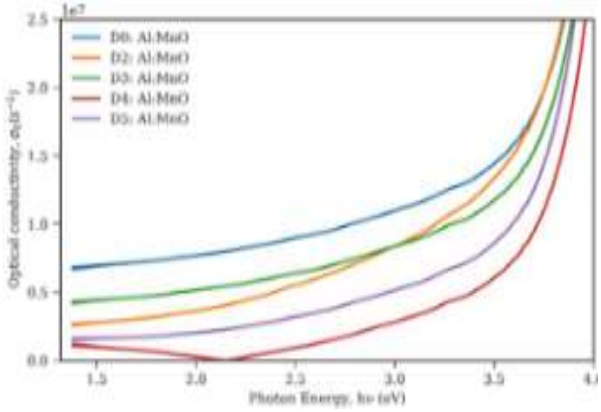


**Fig 8** Plot of optical conductivity versus photon energy for AMO thin film annealed at 300°C for varying time

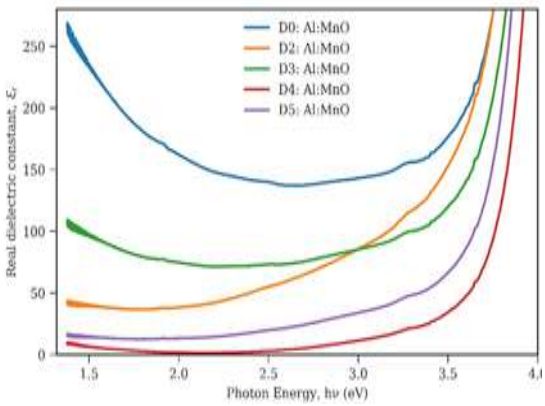


**Fig.9** Plot of Real dielectric constant versus photon for

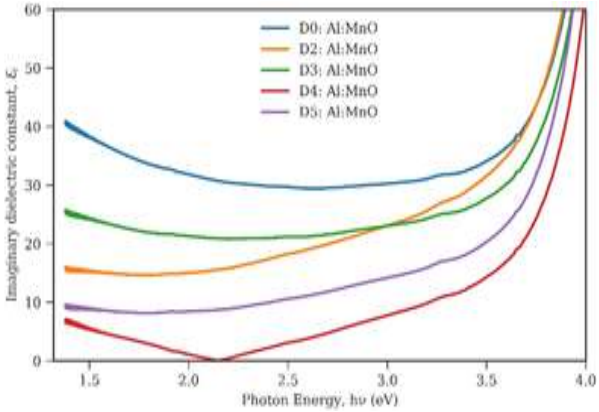


**Fig.10** Plot of imaginary dielectric constant versus photon for AMO thin film annealed at 300°C for varying time

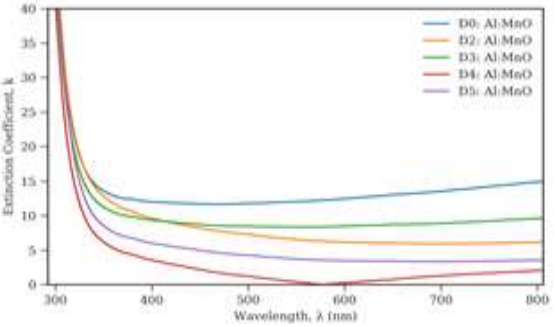


**Fig.11** Plot of extinction coefficient constant versus photon for AMO thin film annealed at 300°C for varying time

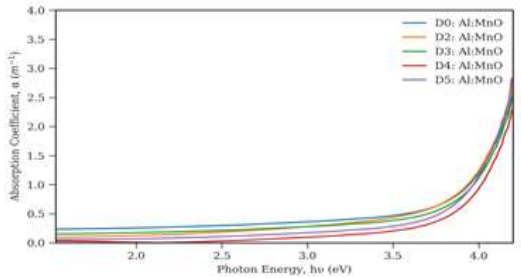


**Fig.12** Plot of absorption coefficient constant versus photon for AMO thin film annealed at 300°C for varying time

## Conclusion

Aluminium doped, MnO thin films were deposited on glass substrates by adopting the conventional low cost SILAR deposition technique. The samples were annealed at 300°C and the anealing time varied from 1hr, 1hr.30mins, 1hr.45mins, 2hrs respectively.

The thin films deposited were characterised to obtain their optical properties such as spectral absorbance, transmittance and reflectance. Other solid state properties like extinction coefficient, imaginary dielectric constant, real dielectric constant, optical conductivty and energy band gaps were also studied. The characterization of these films reveals their potential application in different areas. These include, solar energy collection cover, antireflection coatings, protective coatings, and in electronics.

The structural properties of Al doped manganese oxide [AMO] were characterize using the XRD analysis which revealed that the films are polycrystalline in nature. The crystallite size was found to increase with increase in annealing time. SEM micrograph of the thin films reveals that increase in annealing tempreture time improved the crystallinity of the films with the grain size evenly distributed.

**Funding:** The authors received no funding for this research.

**Data Availability Statement:** The data that support the findings of this study are available on request from the corresponding author.

## Declarations

**Conflict of interest:** None to declare.

**Ethical Statement:** The paper reflects the authors' research and analysis in a truthful and complete manner.

### References


Bellal, S., Hadj, B. & Benrabah, A. K. (2020). Effect of Co doping on the functional properties of $MnO_2$ thin films. *J. Mol. Engine Mater.*, 09: 1-2.

Chougule, M. A., Pawar, S. G., Godse, P. R., Sakhare, R. D., Shashwati, S. & Patil, V. B. (2012). Optical properties of Mn-Co-Ni-O thin films prepared by chemical bath deposition. *J. Mater Sci: Mater Electron*, 3(23): 772.

Chougule.; M. A., Pawar, S. G., Godse, P. R., Sakhare, R. D., Shashwati, S. & Patil, V. B. (2012). Optical properties of Mn- Co-Ni-O thin films prepared by chemical bath deposition. *J. Mater Sci: Mater. Elect.* 3(23): 772.

Gao, Y. Q., Huang, Z. M., Hou, Y. J., Zhou, W., Zhang, L. B. & Chu, J. H. (2014). Infrared optical properties of $Mn1.56Co0.96Ni0.48O_4$ thin films prepared by chemical solution deposition. *Appl. Phys A: Mater Sci Process*, 114: 829-832.

Guotai, Z., Jingse, Z., Yauh, Z., Guical, Q. & Weighing, T. (2019). Synthesis of aluminum doped ion-sieve Manganese oxides powders that enhance adsorption performance. *Colloids and Surfaces A*, 583: 20.

He, L. & Ling, Z. (2011). Studies of temperature dependent ac impedance of a negative temperature coefficient Mn-Co-Ni-O thin film thermistor. *Appl. Phys. Lett.*, 98: 2421121–2421123.

Ilya, E. Paul, S. V., Ilya, M. & Yuru, M. K. (2021). Application of Manganese oxide thin films obtained by ALD for Li-ion batteries anode. *Nano. Res. And. Appl.*, 12: 231-236.

Jaml, H., Khaleeq, M., Rahman, U., Dildar, I. M. & Sarma, S. (2017). Structural and optical properties of Manganese oxide thin films deposited by pulsed laser deposition at different substrate temperature. *Laser Phys J.*, 27: 9.

Mishra, R. K., Prajapati, C. S., Shahi, R. R., Kushwaha, A. K. & Sahay, P. P. (2018). Influence of electrodeposition modes on the electrochemical performance of $MnO_2$ films prepared using anionic $MnO_4$ . (Mn7+) precursor. *Ceramics International*, 44: 5710-5718.

Muslim, Z. & Jiban, P. (2020). Development of semiconductor thin films by spray pyrolysis technique for biosensing application. *Mater. Sci in Semiconductor Processing*, 117: 4.

Osuwa, J. C. & Uwaezi, U. P. (2013). Effects of annealing on the optical, structural and electrical properties of $NiS^2$ thin film. *Chalcogenide Lett.*, 6(8): 385.

Osuwa, J. C., Ezema, F. I. & Oriaku, C. I. (2012). Laser induced changes on band gap and optoelectronic properties of challogenide glashy $CU_{0.11}$ $Cd_{0.40}S_{0.49}$ Thin Films". *J. Non Oxide Glasses*, 2(1): 1-5.

Ozkan, B., Mehmet, E. I. & Harun, G. (2018). Synthesis and characterization of Zn doped $Mn_3O_4$ thin films using SILAR Method. *J Mater Sci: Mater. Electron*, 29: 2.

Park, B. K., Lee, J. W., Lee, S. B., Lim, T. H., Park, S. J. & Park, C.O. (2013). Cu-And Ni doped $Mn1.5Co1.5O_4$ spinel coatings on metallic interconnects for solid oxide fuel cells. *Int. J. Hydrogen Energy*, 38: 12043-12050.

Rajesh, K., Chandra, S. P. & Sahay, P. P. (2018). Super capacitive performance of electrochemically synthesized nanocrystalline $MnO_2$ films using different plating solutions: A comparative study. *J. Alloy. Compounds*, 749: 172-179.

Sahay, P. P. & Ajay, K. K. (2017). Electrochemical supercapacitive performance of potentiostatically cathodic electrodeposited nanostructured $MnO_2$ films. *J. Solid State Electrochem.*, 21: 2393-2405.

Salek, G., Dufour, P., Guillemet-Fritsch, S. & Tenailleau, C. (2015). Sustainable low temperature preparation of $Mn_3{-}xCoxO_4$ ($0 \leq x < 3$) spinel oxide colloidal dispersions used for solar absorber thin films. *Mater. Chem: Phys.*, 162: 252-262.

Sina, K., Babak, S. & Yien-Chien, J. (2023). Emerging atomic layer deposition for the development of high-performance Lithium-ion batteries. *Electrochem. Energy Reviews* 24:6.

Su, X., Yu, L., Cheng, G., Zhang, H., Sun, M. & Zhang, L. (2014). Controllable hydrothermal synthesis of Cu-doped A-$MnO_2$ films with different morphologies for energy storage and conversion using super capacitors. *Apple Energy*, 134: 439-445.

Tadatsugu, M., Yuki, N., Toshihiro, M. & Jun-ichi, N. (2016). High-efficiency oxide solar cells with $ZnO/Cu_2O$ heterojunction fabricated on thermally oxidized $Cu_2O$ sheets. *Appl. Phys. Exp.*, 4: 062301.

Wim, T. (2012). Renewable energy global energy assessment (GEA). Cambridge University Press.